JOURNAL OF MATERIALS SCIENCE 26 (1991) 865–869

Local structural analysis of hopeite crystals by the EXAFS curve-fitting method

NOBORU SATO*, KENJI WATANABE, TATSUO MINAMI
Honda Motor Co. Ltd, Materials Engineering, 1907 Hirata-cho, Suzuka 513, Japan

Structural analysis of hopeite crystals was performed by the extended X-ray absorption fine structure (EXAFS) curve fitting method. Two types of hopeite crystals, $Zn_3(PO_4)_2 \cdot 4H_2O$ and $Zn_{3-x}Mn_x(PO_4)_2 \cdot 4H_2O$ which is doped by manganese, were studied. Fourier transform of EXAFS gave Zn–O bond distances of 0.146 nm for the former and 0.144 nm for the latter. The real bond distances were determined by the reverse operation of Fourier transform and curve-fitting. By this procedure, the real bond distances of Zn–O were determined to be 0.194 and 0.196 nm, respectively. These distances indicated a Zn–O bond in $[ZnO_4]$ of tetrahedral structure. Although the Mn–O bond distance in $Zn_{3-x}Mn_x(PO_4)_2 \cdot 4H_2O$ was found to be 0.162 nm by the Fourier transform of EXAFS, the reverse operation of Fourier transform gave a real bond distance of 0.215 nm for the Mn–O bond in the hopeite crystal. The data supported the idea that the Mn–O bond refered to $[MnO_2(H_2O)_4]$ of the octahedral structure in the crystal. The coordination numbers of the zinc and manganese components clarified their local structure in hopeite crystals.

1. Introduction

Extended X-ray absorption fine structure (EXAFS) is a very useful method by which to analyse the local structure of various kinds of materials. The bond distances between absorbing atoms of X-ray and scattering atoms, or the coordination number of absorbing atoms, in particular, may be clarified by the EXAFS curve-fitting method which is performed as the reverse operation of Fourier transform.

Two types of hopeite crystals-are formed on zinc-coated steels for use as automobile bodies. One is the conventional hopeite ($Zn_3(PO_4)_2 \cdot 4H_2O$), the other is modified hopeite ($Zn_{3-x}Me_x(PO_4)_2 \cdot 4H_2O$) (Me:Mn and/or Ni) [1–12].

Here, $Zn_{3-x}Mn_x(PO_4)_2 \cdot 4H_2O$, the modified hopeite was studied and compared to the conventional hopeite, because the manganese component is more important than the nickel with regard to the durability against corrosion [1, 6].

EXAFS was applied to clarify the crystalline structure for these materials, because EXAFS data can elucidate detailed structure, such as the manganese position in the crystals.

2. Materials and methods

2.1. Hopeite crystal samples

Two kinds of hopeite crystals were studied: one without manganese (hopeite A) and the other with a manganese component (hopeite B)

$Zn_3(PO_4)_2 \cdot 4H_2O$ hopeite A (Zn 42.6 wt %)

$Zn_{3-x}Mn_x(PO_4)_2 \cdot 4H_2O$ hopeite B (Zn 38.0 wt %; Mn 4.8 wt %)

Metallic component compositions were determined by atomic absorption spectroscopy using a Hitachi 180-60 instrument.

2.2. Analysis by EXAFS

The EXAFS instrument at the National Laboratory for High Energy Physics was used under the following conditions.

1. Absorbing edges: Zn*K* and Mn*K* crusts.
2. Monochromator:
   Si (3 1 1) channel cut
   Dual crystal monochromator
   Lattice constants $d = 0.163\,747$ nm
   Plane spacing $D = 9.5$ mm.
3. Measurement by the penetration system at room temperature.
4. Beam line: BL10B.

In general, the vibrational structure $\chi(K)$ of EXAFS is expressed by Equations 1 and 2 [13]

$$\chi(K) = A(K)\sin[2KR + \phi(K)] \quad (1)$$

$$A(K) = NS(K)|f(K, \pi)|\exp(-2\sigma^2K^2)/KR^2 \quad (2)$$

N is the coordination number of the scattering atom, K is the wavenumber expressed as $2\pi/\lambda$ (λ = wavelength), $S(K)$ is the damping parameter, $|f(K, \pi)|$ is the back-scattering factor, σ is the Debye–Waller factor, R the bond distance and $\phi(K)$ the deviation of phase shift caused by interactions between absorption atoms and scattering atoms. KR^2 refers to the extending degree of electrons with a spherical wave condition.

* *Present address*: 11 Laboratory, Honda Wako Research Center, 1-4-1, Chuo, Wako, 351-01, Japan.

0022–2461/91 $03.00 + .12

When the vibrational structure of EXAFS is analysed, Fourier transform of Equation 3 is performed, because the structure would become complicated by the summation of atoms which have different bond lengths. Fourier transform of EXAFS implies a radial distribution of an atom and provides some information about environmental conditions for the atoms.

$$F(R) = [1/(2\pi)^{\frac{1}{2}}] \int_{K_{min}}^{K_{max}} K^n \chi(K) \exp(-2iKR) dK \quad (3)$$

where K_{max} and K_{min} refer to the wavenumber region of Fourier transform. Coefficient, K^n to emphasize $\chi(K)$ is performed for Fourier transform of Equation 3. The radial distribution $F(R)$, which has a peak in $R' = R + \phi(K)$, is obtained by this procedure.

However, the Fourier transform contains a deviation $\phi(K)$ of phase shift as shown in Equations 1 to 3. Therefore, the bond distances obtained by these procedures do not indicate the real values. It is necessary to correct the deviation of phase shift to investigate the real distances. For that purpose, the reverse operation of Fourier transform should be carried out.

The reverse operation of Fourier transform from R space to K space is expressed by

$$K^n \chi(K) = [1/(2\pi)^{\frac{1}{2}}] \int_{R_{min}}^{R_{max}} W(R) F(R) \exp(2iKR) dR \quad (4)$$

$$W(R) = \begin{cases} 1 - \cos[\pi(R - R_{min})/D]/2 \\ 1 \\ 1 - \cos[\pi(R_{max} - R)/D]/2 \end{cases}$$

$$\begin{aligned} &R_{min} < R < R_{min} + D \\ &R_{min} + D < R < R_{max} - D \\ &R_{max} - D < R < R_{max} \\ &(D \approx 0.01 \text{ nm}) \end{aligned} \quad (5)$$

After correction of the phase shift $\phi(K)$, $\chi(K)$ is calculated from Equation 3. Then, the best N, R and σ which can explain $\chi(K)$, found by experiment are determined by the curve-fitting method.

3. Results and discussion

3.1. Zinc component analysis

Fourier transform of EXAFS related to the zinc components in hopeite A and B was carried out using Equation 3, and is shown in Fig. 1. The radial distributions of the first neighbouring atoms appeared at a distance of 0.146 nm for hopeite A and at 0.144 nm for hopeite B [10]. The peaks of hopeite B were smaller than those of hopeite A, because the local structure of the zinc component was disordered by the manganese component in hopeite B. It was thought that the local structure of the zinc component became complicated by the manganese coordination in the crystals.

As an example, the reverse operation of Fourier transform was performed for the first peak of hopeite A in Fig. 1 and the curve-fitting method, which is able to explain the best N, R and σ, was performed. The

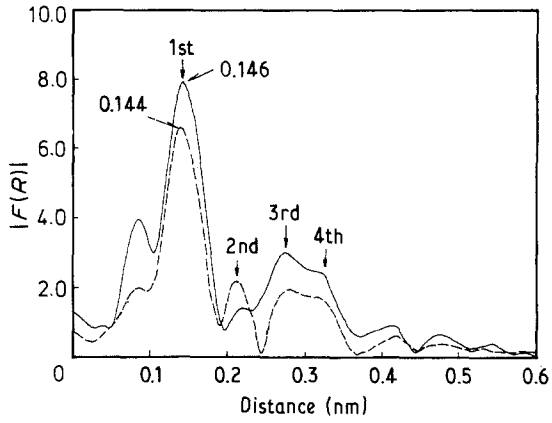

Figure 1 Fourier transforms of EXAFS showing ZnK absorption edges of hopeite (—) A and (– – –) B.

results are shown in Fig. 2. Here, K^n for $\chi(K)$ was treated as $n = 3$.

Figs 2 and 3 show the results for the first peaks of hopeite A and B, and Figs 4 and 5 those for the second peaks of hopeite A and B.

When the first neighbouring atoms in Figs 2 and 3 were assumed to be oxygen, the curve fitting was quite good. When the atoms of the second peaks in Figs 4 and 5 were assumed to be phosphorus, the curve fitting was also satisfactory.

These data imply the distance of Zn–P position. When the second peaks were assumed to be Zn–O,

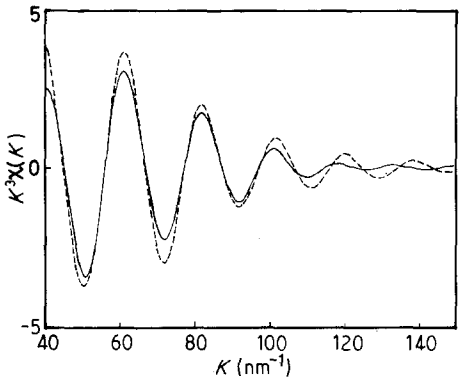

Figure 2 Reverse operation of Fourier transform and curve fitting for the first peak of hopeite A. (—) Experimental values, (– – –) calculated values.

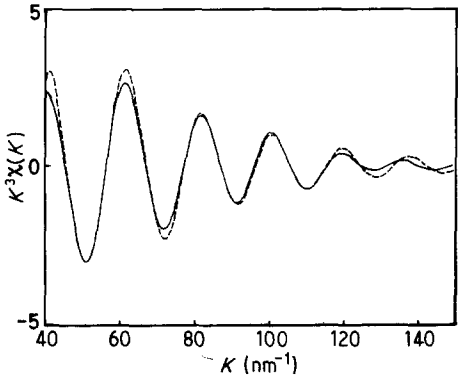

Figure 3 Reverse operation of Fourier transform and curve fitting for the first peak of hopeite B. (—) Experimental values, (– – –) calculated values.

TABLE I Bond distances and coordination numbers for Hopeite A and B determined by the curve-fitting method

Peak obtained by Fourier transform	Bond	Distance, R (nm)		Coordination number, N	
		Hopeite A	Hopeite B	Hopeite A	Hopeite B
1st	Zn–O	0.194 (0.211, 0.195)* (0.210, 0.196)†	0.196	4.0	3.1
2nd	Zn–P	0.254	0.250	0.5	0.9
3rd	Zn–P	0.317	0.318	4.1	2.1
4th	Zn–P	0.361	0.361	2.7	2.1

* Crystallographic data from Hill [16]. † Crystallographic data from Whitaker [14].
† 0.211 and 0.210 nm: Zn(1)–O in $[ZnO_2(H_2O)_4]$.
0.195 and 0.196 nm: Zn(2)–O in $[ZnO_4]$.

Zn–Zn, or Zn–Mn, the results were not good. In the same way, the position of Zn–P for the third and fourth peaks could be explained.

Table I gives a summary of these data. Here, the resolving power of distance R was about 0.005 nm, and that of the coordination number was about 1. Accordingly, the bond distances were almost the same in the two types of hopeite crystals. However, there is a difference of $\sim$ 0.05 nm between the distances (0.146 or 0.144 nm) obtained by Fourier transform in Fig. 1, and the results in Table I (0.194 or 0.196 nm) for the phase shift deviation, $\phi(K)$, shown in Equation 1 have been corrected.

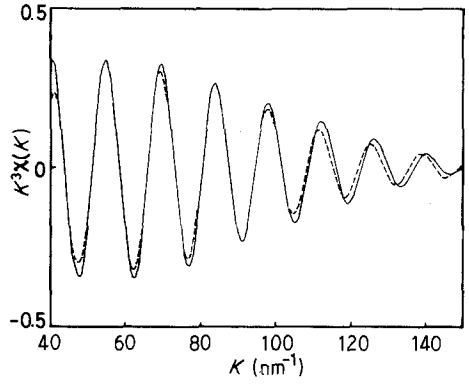

Figure 4 Reverse operation of Fourier transform and curve fitting for the second peak of hopeite A. (—) Experimental values, (– – –) calculated values.

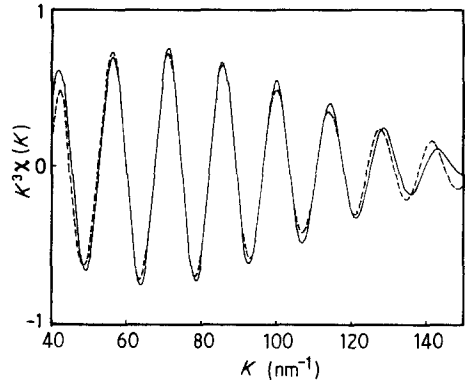

Figure 5 Reverse operation of Fourier transform and curve fitting for the second peak of hopeite B. (—) Experimental values, (– – –) calculated values.

The zinc components in hopeite crystals are considered to be tetrahedral $[ZnO_4]$ and octahedral $[ZnO_2(H_2O)_4]$. These chemical structures and the unit cell of the hopeite crystals are shown in Fig. 6 [14]. The zinc components of the octahedral and the tetrahedral structures are expressed as Zn(1) and Zn(2), respectively. Hill and Jones [15] reported that the average bond distances of Zn(1)–O and Zn(2)–O were 0.211 and 0.195 nm, respectively, by means of crystallographic investigation [15]. Whitaker reported almost the same values [14]. Because the bond distances of Zn–O for the first peaks in Table I were 0.194 nm for hopeite A and 0.196 nm for hopeite B, these data signify a Zn(2)–O bond in the $[ZnO_4]$ tetrahedron. In fact, curve fitting was not suitable for the Zn(1)–O bond in the octahedral structure. The fact that the coordination number for the zinc component of the first peak in hopeite A was 4, also implies Zn(2)–O bond in the $[ZnO_4]$ tetrahedral structure. On the contrary, the coordination number for hopeite B with a manganese component was 3.1.

In phosphophyllite crystals $(Zn_2Fe(PO_4)_2 \cdot 4H_2O)$, the zinc component in the $[ZnO_2(H_2O)]$ octahedral structure is substituted by an iron component: $[FeO_2(H_2O)_4]$ [16]. When the manganese component is coordinated in the hopeite crystal structure, it is thought that $[MnO_2(H_2O)_4]$ octahedral structure could be formed such as with the iron component. In the latter case, all the octahedral structures form $[FeO_2(H_2O)_4]$; however, the manganese component partially substitutes for the zinc component in the octahedral structure, e.g. $Zn_{3-x}Mn_x(PO_4)_2 \cdot 4H_2O : 0 < x < 1$.

Accordingly, because the manganese component which is coordinated in the octahedral structure of the hopeite crystals does not affect the $[ZnO_4]$ tetrahedral

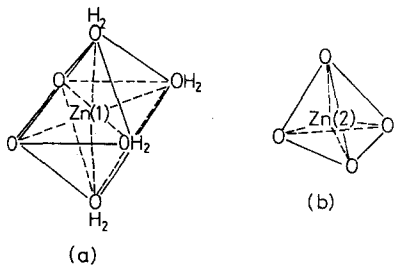

Figure 6 Chemical structure and unit cell of hopeite crystals.

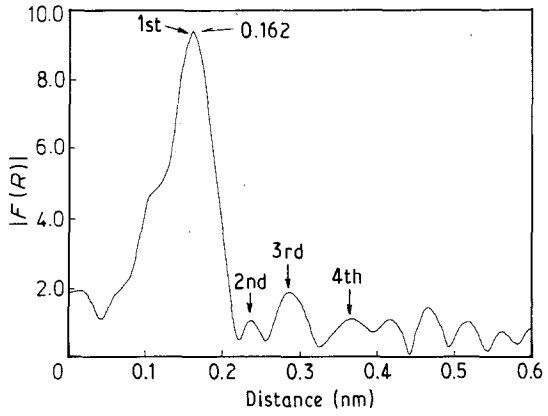

Figure 7 Fourier transform of EXAFS showing Mn*K* absorption edge of hopeite B.

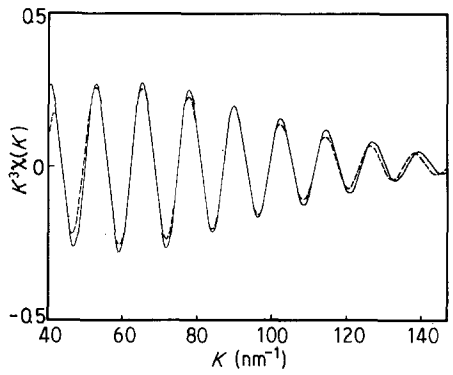

Figure 9 Reverse operation of Fourier transform and curve fitting for the second peak of hopeite B. (—) Experimental values, (---) calculated values.

structure, the coordination number of zinc for the first peak of hopeite B should be interpreted as 4. These experimental data are thought to be reasonable because the resolving power for the coordination number is approximately 1.

3.2. Manganese component analysis

Fourier transform of EXAFS for the Mn*K* absorption edge in hopeite B ($Zn_{3-x}Mn_x(PO_4)_2 \cdot 4H_2O$) is shown in Fig. 7. The first peak appeared at 0.162 nm. The reverse operation of Fourier transform and curve fitting are shown in Fig. 8. In the same way, that for the second peak is shown in Fig. 9. Table II gives a summary of these data.

Because the first manganese peak showed an Mn–O distance of 0.215 nm, it confirmed that the manganese component substituted for zinc component in the octahedral structure as shown in Fig. 10.

This is supported by the data of the coordination number. If the manganese component substituted for the zinc component in the tetrahedral structure, the coordination number for the first manganese peak would be ~ 4. On the contrary, if the manganese component substituted for the zinc component in the octahedral structure, the number would be ~ 6. The curve-fitting method gave a value of 6.8, which should be interpreted as 6, due to the resolving power.

TABLE II Bond distances and coordination number for Hopeite A and B determined by the curve-fitting method

Peak obtained by Fourier transform	Bond	Distance, R (nm)	Coordination number, N
1st	Mn–O	0.215	6.8
2nd	Mn–P	0.277	0.5
3rd	Mn–P	0.341	3.2
4th	Mn–P	0.405	4.6

These data support the idea that the manganese component is coordinated to the octahedral structure, forming $[MnO_2(H_2O)_4]$ with a chemical structure of $Zn_{3-x}Mn_x(PO_4)_2 \cdot 4H_2O$.

4. Conclusions

1. For hopeite crystals of $Zn_3(PO_4)_2 \cdot 4H_2O$ and $Zn_{3-x}Mn_x(PO_4)_2 \cdot 4H_2O$, the radial distribution of EXAFS of the latter was smaller than that of the former, because the local structure of the zinc component became complicated by the action of the manganese component.

2. In the Fourier transforms of EXAFS, oxygen, which is the first neighbouring atom to the zinc component, showed peaks at a distance of 0.146 and 0.144 nm. However, the real bond distances for Zn–O

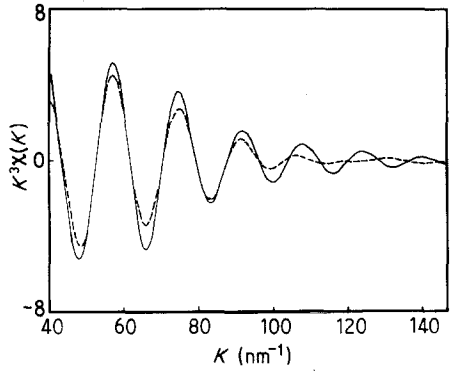

Figure 8 Reverse operation of Fourier transform and curve fitting for the first peak of hopeite B. (—) Experimental values, (---) calculated values.

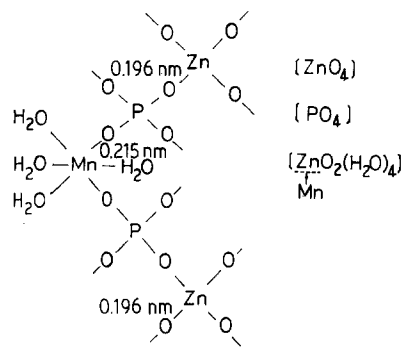

Figure 10 Chemical structure of hopeite B containing a manganese component.

determined by the reverse operation of Fourier transform were 0.194 and 0.196 nm, respectively. Therefore, there is a difference of ~ 0.05 nm between these values.

3. The real bond distances by curve-fitting method showed good consistence with crystallographic data. And it was confirmed that first peak shown in Fourier transform of EXAFS corresponded to Zn–O bond and second peak of that corresponded to Zn–P position.

4. The coordination number, N, and bond distance, R, obtained by the curve-fitting method clarified that the first peak of Fourier transform was due to the Zn–O bond in the $[ZnO_4]$ structure which is the basic component of hopeite crystals.

5. In the Fourier transform of EXAFS, oxygen which is the first neighbouring atom for the manganese component in $Zn_{3-x}Mn_x(PO_4)_2 \cdot 4H_2O$ showed a peak at a distance of 0.162 nm. However, the real bond distance of Mn–O was determined as 0.216 nm from the reverse operation of Fourier transform.

6. Data for the real bond distance of Mn–O and the coordination number of manganese supported the idea that the manganese component in hopeite crystals was coordinated with the octahedral structure with a chemical state of $[MnO_2(H_2O)_4]$.

7. Fourier transform and its reverse operation, including curve fitting, were very useful in clarifying the hopeite crystal structure, especially the coordination state of the manganese component in $Zn_{3-x}Mn_x(PO_4)_2 \cdot 4H_2O$.

References

1. N. SATO, *Surf. Coat. Technol.* **30** (1987) 171.
2. *Idem, J. Metal Finishing Soc. Jpn* **37** (1986) 758.
3. N. SATO and T. MINAMI, *ibid.* **38** (1987) 30.
4. *Idem, ibid.* **38** (1987) 108.
5. *Idem, ibid.* **38** (1987) 149.
6. N. SATO, T. MINAMI and H. KONO, *ibid.* **38** (1987) 571.
7. *Idem, Surf. Coat. Technol.* **37** (1989) 23.
8. T. MINAMI and N. SATO, *J. Surf. Sci. Jpn* **9** (1988) 459.
9. N. SATO and T. MINAMI, *J. Chem. Soc. Jpn* **1988** (1988) 1891.
10. T. MINAMI and N. SATO, *ibid.* **1988** (1988) 1741.
11. N. SATO and T. MINAMI, *J. Mater. Sci.* **24** (1989) 4419.
12. N. SATO, Dr. thesis, The University of Tokyo (1988).
13. B. K. TEO and D. C. JOY, "EXAFS Spectroscopy" (Plenum Press, New York, London, 1980) p. 1.
14. A. WHITAKER, *Acta. Crystallogr.* **B31** (1975) 2026.
15. R. J. HILL and J. B. JONES, *Amer. Mineral.* **61** (1976) 987.
16. R. J. HILL, *ibid.* **62** (1977) 812.

Received 17 August 1989
and accepted 19 February 1990